ELSEVIER

Journal of Hazardous Materials B122 (2005) 129–138

Journal of Hazardous Materials

www.elsevier.com/locate/jhazmat

Vitrified metal finishing wastes
II. Thermal and structural characterisation

P.A. Bingham [a,*], R.J. Hand [a], S.D. Forder [b], A. Lavaysierre [b]

[a] *Immobilisation Science Laboratory, Department of Engineering Materials, University of Sheffield, Mappin Street, Sheffield S1 3JD, UK*
[b] *Materials and Engineering Research Institute, Sheffield Hallam University, Howard Street, Sheffield S1 1WB, UK*

Received 21 December 2004; received in revised form 1 March 2005; accepted 14 March 2005
Available online 22 April 2005

Abstract

Waste filter cakes from two metal finishing operations were heat treated and vitrified. Substantial weight loss during heating was due to emission of water, volatile sulphur-rich and chlorine-rich compounds, and the combustion of carbonaceous components. Estimations of CO_x, SO_x and HCl emissions were based on chemical analyses. Upon cooling from molten, one sample remained amorphous but all others partially crystallised. Crystalline nature was dependent upon waste composition and the level of P_2O_5 addition. Thermal stabilities of the waste forms were good, but less so than MW, a borosilicate glass developed for its high temperature stability. Mössbauer and FTIR analyses showed that iron environments in the different vitrified waste forms were very similar. Iron was present predominantly as Fe^{3+}, although the exact redox ratio varied slightly between waste forms. Iron in both redox states occupied distorted octahedral coordination polyhedra with similar levels of site distortion. Phosphate networks in the vitreous materials were highly de-polymerised, consisting largely of $(PO_4)^{3-}$ monomer and $(P_2O_7)^{2-}$ dimer units. This explained the high chemical durability of these waste forms and their structural insensitivity to compositional change, underlining their suitability as hosts for the immobilisation of toxic and nuclear wastes.

Keywords: Glass; Vitrification; Phosphate; Waste; Structure

1. Introduction

Previously we discussed the treatment of filter cake samples from two metal finishing operations in terms of the chemical composition, density and chemical durability of dried, sintered and vitrified waste forms [1]. The heat treated wastes and the vitrified wastes had high chemical durability and would be safe for landfill or, preferably, for re-use in a number of potential applications. Vitrification is an established method for volume reduction and inertisation of solid municipal and industrial wastes [2], and vitrified wastes are used in an increasing number of applications, for example as glass fibres [3–5]. The two metal finishing wastes we have studied consisted largely of zinc, iron and phosphorus compounds, their exact makeup varying with waste source [1]. Oxide glasses based on these three components typically have good chemical durabilities, low melting temperatures, low coefficients of thermal expansion and high waste-loading capabilities. They have therefore attracted attention as potential host matrices for the immobilisation of certain nuclear wastes [4,6–9]. Although the strengthening of environmental legislation in recent years encourages consideration of vitrification as a method of waste immobilisation, said legislation also places strict emissions limits on the high temperature processing of waste. Hence emissions of CO_2, NO_x, SO_x, HCl and particulates are tightly controlled for processes involving the vitrification or incineration of wastes [10].

2. Experimental procedure

Filter cake samples were taken from two metal finishing operations, and were named waste B and waste P. Full

* Corresponding author. Tel.: +44 114 2225473; fax: +44 114 2225943.
E-mail address: p.a.bingham@sheffield.ac.uk (P.A. Bingham).

0304-3894/$ – see front matter © 2005 Elsevier B.V. All rights reserved.
doi:10.1016/j.jhazmat.2005.03.031

Table 1
Summary of normalised material compositions by EDS, ICP-OES and Leco analyses in weight %

Component	Analysis technique	Sample B-1	Sample B-2	Sample B-3	Sample B-4	Sample P-1	Sample P-2	Sample P-3	Sample P-4
		Dried, 18 h, 120 °C	Heated, 1 h, 1000 °C	Vitrified, 1 h, 1100 °C	Vitrified, 1 h, 1100 °C	Dried, 18 h, 120 °C	Heated, 1 h, 1000 °C	Vitrified, 1 h, 1100 °C	Vitrified, 1 h, 1100 °C
H_2O	L.o.d.	22.7	–	–	–	44.3	–	–	–
C	Leco	5.9	–	–	–	4.2	–	–	–
Na_2O	ICP-OES	2.0	2.0[a]	1.2[a]	1.0[a]	4.9	4.9[a]	4.4[a]	3.9[a]
MgO	EDS	0.2	0	0	0	0	0	0	0
Al_2O_3	EDS	0.1	0	0.8	0.6	2.6	5.8	1.8	3.3
SiO_2	EDS	1.3	1.4	1.1	1.2	0.5	0	0	0
P_2O_5	EDS	3.9	2.2	35.5	43.7	36.2	32.8	43.8	51.0
SO_3	EDS (Leco)	1.4	0.9	0.3 (0.02)	0.4 (0.05)	0.8	0.2 (0.04)	0.4 (0.03)	0.4 (0.03)
Cl	EDS	4.1	0	0	0	0	0	0	0
K_2O	EDS	0.2	0.2	0.1	0.2	0.8	0.8	0.7	0.6
CaO	EDS	0.2	0.3	0.2	0.3	1.6	2.6	2.1	1.8
TiO_2	EDS	0	0	0	0	0.6	0	0.5	0.4
Cr_2O_3	EDS	2.1	2.1	1.4	1.4	0	0	0	0
MnO	EDS	0.3	0.8	0.5	0.4	2.3	2.9	2.2	2.3
Fe_2O_3	EDS	28.1	28.4	19.7	18.3	40.6	39.7	35.5	32.1
NiO	EDS	0.3	0.3	0.3	0.2	0.8	1.5	1.0	0.9
ZnO	EDS	55.8	61.5	39.0	32.6	8.3	8.8	7.7	6.5

The data given in the second row of header are treatments.
[a] Estimated percentages based on ICP-OES analyses of samples B-1 and P-1.

details of their compositional analyses and treatments were given previously [1], and they have been summarised here in Table 1. Analysis methods were energy-dispersive X-ray spectroscopy (EDS), inductively-coupled plasma spectroscopy (ICP) and Leco induction furnace combustion analysis. Both wastes underwent a range of heat treatments: drying at 120 °C (samples B-1 and P-1); heat treatment at 1000 °C (samples B-2 and P-2); or addition of two levels of P_2O_5 precursor material with subsequent vitrification at 1100 °C (samples B-3, B-4, P-3 and P-4) [1].

X-ray diffraction (XRD) spectroscopy was carried out using a Philips PW1730/10 goniometer with Co Kα radiation. Spectra were measured at a rate of 0.1° 2θ/min between 10° and 80° 2θ.

Differential thermal analysis (DTA) was performed using a Perkin-Elmer DTA 7. Powdered glass samples weighing 25 mg and with a particle size of <75 μm were placed in recrystallised Al_2O_3 sample cups and heated at 10 °C/min from room temperature to 1200 °C.

Thermogravimetric analysis (TGA) was carried out using a Perkin-Elmer Pyris 1. Powdered glass samples with a particle size of <75 μm and weighing from 2 to 6 mg were placed in recrystallised Al_2O_3 sample cups and heated from room temperature to 1000 °C at 10 °C/min. Prior to measurement, waste samples were dried at 120 °C for 18 h.

Mössbauer spectroscopy was carried out at room temperature using an in-house spectrometer with a 25 mCi ^{57}Co source embedded in a Rh matrix. The absorbers were prepared from ground glass mixed with graphite powder to ensure a Mössbauer thickness $t < 1$ [11]. Spectra were measured in the velocity range −5 to +5 mm s^{-1} in constant acceleration mode. Calibration of the spectrometer was made using α-Fe. Seven and eight broadened Lorentzian paramagnetic doublets were fitted to the spectra obtained on samples P-4 and B-4, respectively, using the Recoil analysis software package [12].

Fourier-transform infrared (FTIR) spectroscopy was performed using a Perkin-Elmer Spectrum 2000 spectrometer with a fixed-angle specular reflectance unit at 16° incidence. Kramers–Kronig transformations were carried out by software. Background spectra were measured prior to each sample and all spectra were averaged over 20 measurements. Spectra were measured between 400 cm^{-1} and 1400 cm^{-1} at 4 cm^{-1} resolution and 1 cm^{-1} data interval.

3. Results

3.1. X-ray diffraction (XRD)

Only one sample, P-4, produced an entirely amorphous XRD spectrum, and partially amorphous samples B-3, B-4, P-2 and P-3 exhibited some crystallisation on cooling. XRD spectra measured for samples P-1 to P-4 are shown in Fig. 1 and spectra for samples B-1 to B-4 in Fig. 2. Established crystal phases are detailed in each figure.

3.2. Thermogravimetric analysis (TGA)

Measured weight losses and derivatives thereof, obtained using a 20-point moving average analysis, are shown in Fig. 3. Weight losses up to 500 °C were approximately 15–20% for both wastes, and with similar rates of loss. Both samples exhibited particularly strong losses between 500 °C and 600 °C.

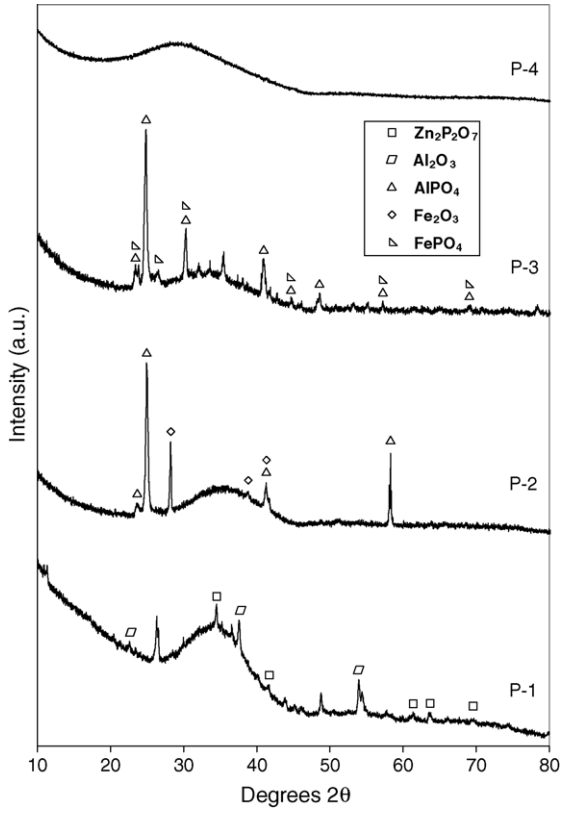

Fig. 1. XRD spectra for samples P-1 to P-4.

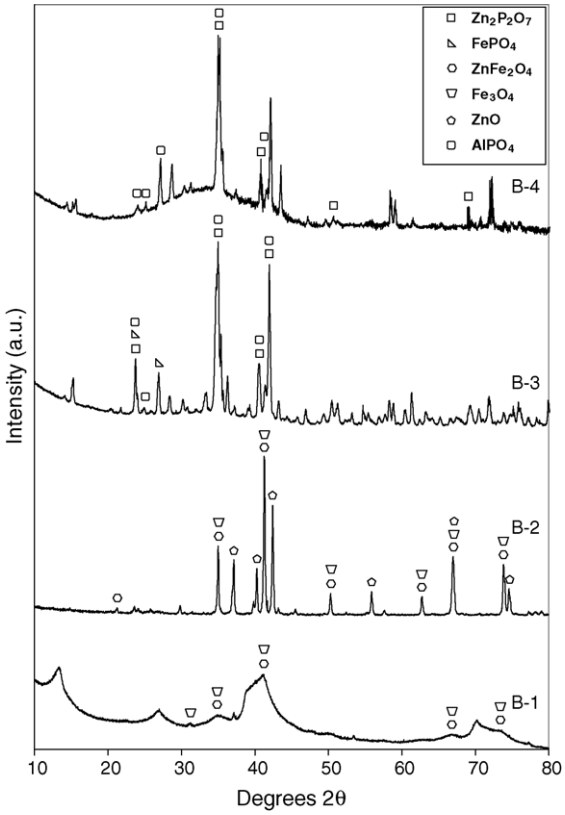

Fig. 2. XRD spectra for samples B-1 to B-4.

Waste B continued to lose weight up to 1000 °C, whereas the weight of waste P remained approximately constant above 650 °C. Total weight losses from the two wastes were 20% from waste P and 27% from waste B.

3.3. Differential thermal analysis (DTA)

DTA investigated the crystallisation and melting behaviour of samples B-4, P-2, P-4 and MW over the temperature range 20–1200 °C. Samples B-4 and P-4 were the most amorphous materials produced from their respective wastes, hence they were selected for detailed analysis. Sample P-2 was also studied since it formed a molten liquid with no P_2O_5 addition and remained substantially amorphous upon cooling. Glass MW was measured for comparison as in [1]. Traces are shown in Fig. 4. Samples B-4, P-2 and P-4 exhibited a small endothermic peak at 460–510 °C, broad exothermic peaks in the range

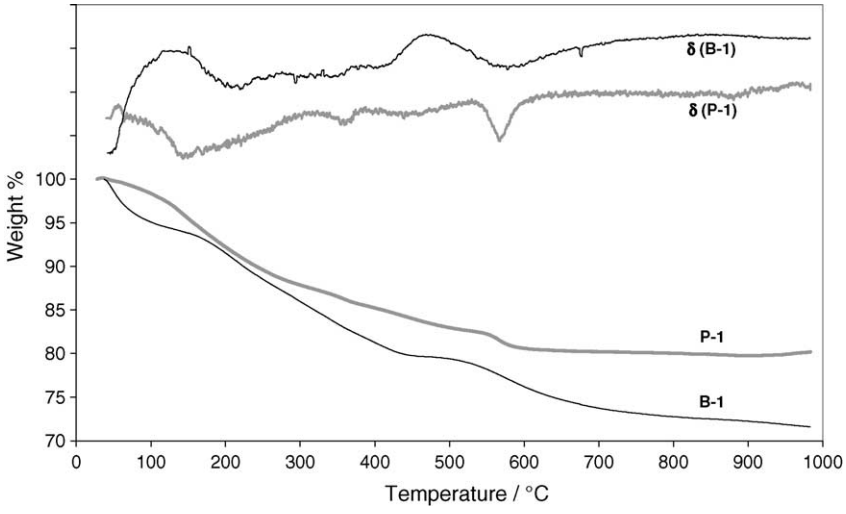

Fig. 3. TGA weight loss and derivative curves of dried waste samples B-1 and P-1.

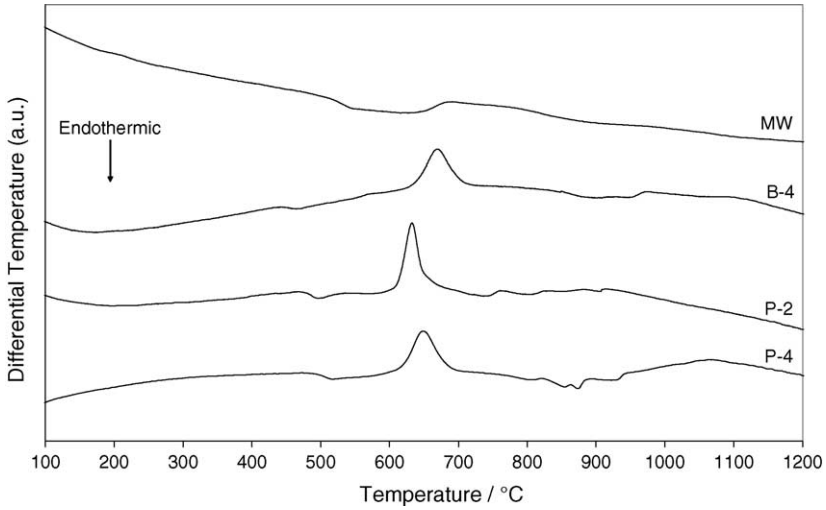

Fig. 4. DTA traces of selected waste forms.

635–675 °C and a number of small peaks in the range 740–950 °C.

3.4. Fourier-transform infra-red (FTIR) reflectance spectroscopy

FTIR reflectance spectra were collected on polished sections of each sample. Only sample P-4 was totally amorphous, so spectra for the other samples may not have been fully representative of each material. Direct comparisons between samples were therefore made with caution. Fig. 5 shows Kramers–Kronig corrected FTIR reflectance spectra which were composed of a number of overlapping absorption bands in the range 400–1400 cm^{-1}. These spectra were consistent with FTIR spectra for many other phosphate-based glasses [4,6–8,13–31].

3.5. Mössbauer spectroscopy

Fitted Mössbauer spectra are shown in Fig. 6, with accompanying parameters in Table 2. Six or eight Lorentzian doublets have previously been fitted to Mössbauer spectra for similar phosphate glasses [4,7,8,14,16,20]. Eight doublets were fitted to the spectrum for sample B-4 and seven to P-4. No statistical improvement was obtained in fitting an eighth doublet to the spectrum of sample P-4 and therefore this was not done. The values of centre shift, quadrupole splitting and linewidth for each valence state were obtained by taking a weighted average from the parameters of each fitted doublet based on their area. The $Fe^{2+}/\sum Fe$ ratio was calculated from the site populations; however, it was assumed that the recoil-free fractions of Fe^{2+} and Fe^{3+} ions were unequal at room temperature in these materials. The redox ratio $Fe^{2+}/\sum Fe$ was calculated by assuming the Fe^{3+} recoil-free

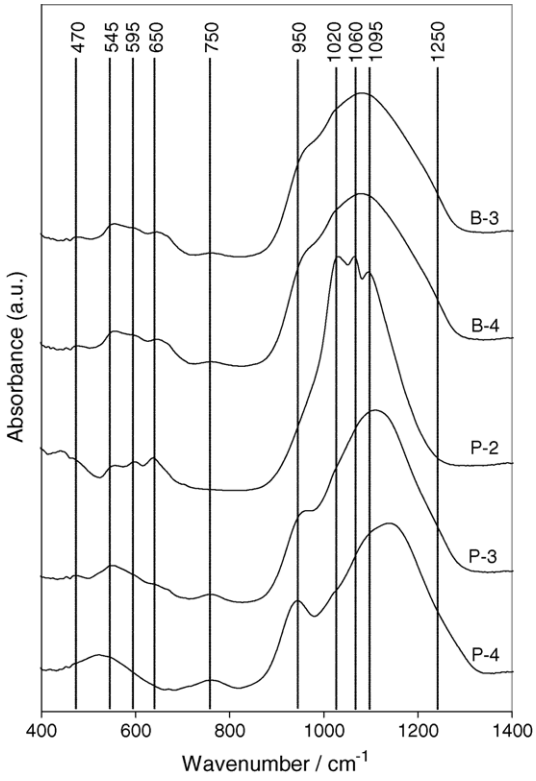

Fig. 5. FT-IR reflectance spectra.

Table 2
Mössbauer hyperfine parameters

	CS Fe^{2+} ($mm\,s^{-1}$)	CS Fe^{3+} ($mm\,s^{-1}$)	QS Fe^{2+} ($mm\,s^{-1}$)	QS Fe^{3+} ($mm\,s^{-1}$)	LW Fe^{2+} ($mm\,s^{-1}$)	LW Fe^{3+} ($mm\,s^{-1}$)	$Fe^{2+}/\sum Fe$ (%)
P-4	1.01	0.41	2.68	0.80	0.16	0.15	11.2
B-4	1.02	0.43	2.67	0.81	0.16	0.15	18.4

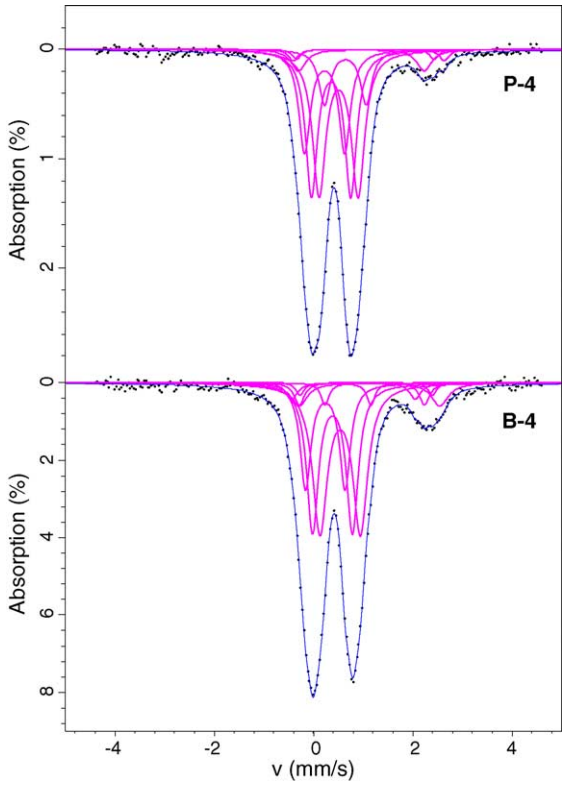

Fig. 6. Mössbauer spectra.

fraction was 1.30 times larger than that of Fe^{2+}. This factor was based on experimentally determined recoil-free fractions from low temperature studies of iron in phosphate glasses [32–35].

The combined error introduced by measurement and fitting was estimated as $\pm 0.02\,\mathrm{mm\,s^{-1}}$ for centre shift, quadrupole splitting and linewidth of both redox states. Errors in the redox ratio were estimated at $\pm 1\%$ $Fe^{2+}/\sum Fe$. Centre shift (CS) is determined by the s-electron density at the Fe nucleus and is therefore a measure of bond covalency and the number and nature of ligands [36]. Quadrupole splitting (QS) is the interaction of the nuclear quadrupole moment with the electric field gradient at the Fe nucleus. For high-spin Fe^{3+} ions the electrons are spherically symmetrical, so only distortions from cubic symmetry contribute to QS and hence it is a direct measure of site distortion. Values of QS (Fe^{2+}) are larger than QS (Fe^{3+}) owing to lack of symmetry caused by the additional electron in Fe^{2+}. Linewidth (LW) is governed by variations in site parameters. It is therefore a measure of the range of site distortions, as opposed to the average site distortion which can be assessed from QS.

3.6. Atmospheric emissions by mass balance

Whilst direct emissions measurements were not made in this study, it was possible to estimate the levels of emitted gases based on chemical analyses of the materials before and after heat treatment, shown in Table 1. Vitrification of the two wastes resulted in materials containing essentially zero chloride and sulphate, and carbon combusted to form CO or CO_2 during treatment. Therefore we assumed that all of the carbon, sulphur and chloride initially present in these wastes were released to the atmosphere as CO, CO_2, SO_2 and HCl, respectively. Simple calculations were then carried out using

$$W(y) = W(z)\,\mathrm{RMM}\left(\frac{y}{z}\right), \quad (1)$$

where $W(y)$ is the weight of gaseous product (CO, CO_2, SO_2 or HCl) emitted, $W(z)$ the weight of C, SO_3 or Cl present in the waste, and RMM(y/z) is the relative molecular mass of the gaseous product/relative molecular mass of the precursor in the waste. Using Eq. (1) and the data from Table 1, we estimated that atmospheric emissions resulting from formation of samples P-4 and B-4 from samples P-1 and B-1 would result in the direct emission of the equivalent of 0–98 kg CO, 0–154 kg CO_2, 6.4 kg SO_2 and zero HCl from waste P, and 0–137 kg CO, 0–216 kg CO_2, 11.2 kg SO_2 and 42 kg HCl from waste B per tonne of waste processed.

4. Discussion

Previously we concluded that waste P was more suitable for direct vitrification than waste B due to its higher phosphate content and preferable melting behaviour [1]. The TGA curves and derivatives shown here in Fig. 3 confirmed the gentler nature of waste P. Its total weight loss was substantially lower than waste B and almost all weight loss took place below 600 °C. Weight loss was approximately linear in the range 200–400 °C, and has widely been attributed to the evolution of H_2O, CO and CO_2 [37–39]. Weight losses levelled off at 450–500 °C then increased again above 550 °C for both samples. It appeared likely that this was due, at least in part, to further combustion of carbonaceous components as occurred during thermal treatment of electroplating sludge, where combustion of the carbonaceous components produced measurable levels of CO_2 particularly above 500 °C, but no CO was detected at any temperature up to 1450 °C [40]. Although the electroplating waste originated from a different process, its chemical composition and heat treatment conditions were not greatly different from wastes B and P, and thus although we have indicated the range of possible CO and CO_2 emissions above it is probable all the carbon in our wastes would combust to form only CO_2 and not CO and this is assumed in the following discussion. However, further work would be required to confirm this assumption. Weight loss can also occur at 500 °C due to decomposition of sulphates [41]. Sulphate contents of our wastes were below 1.5%, but sulphate content of the heat treated wastes were much lower than this. As shown in Table 1, approximately half the sulphate was driven off from waste B and almost all sulphate was evolved from waste P during heating to 1000 °C. We assumed that the sulphur in both wastes occurred largely as iron or zinc sulphates with the ratio between the two vary-

ing with composition. The relatively sharp weight loss from both samples at 500–600 °C may therefore be attributable to a combination of sulphate decomposition [41] and CO_2 liberation [37]. Decomposition of $Fe_2(SO_4)_3$ and $FeSO_4$ takes place at 500–600 °C, whereas decomposition of $ZnSO_4$ occurs at 700–900 °C [41]. Sample B-1 was richer in zinc than P-1, so sulphate decomposition may have occurred over a broader temperature range. This was commensurate with the weight loss behaviour of sample B-1 above 500 °C, and its continued weight loss at temperatures above 700 °C. Full confirmation of these hypotheses would require further studies. Chloride evolution, presumably as HCl [1], also occurred during heating of sample B-1, but no specific TGA peak could be attributed to it. This may contribute to the weight loss from sample B-1 at high temperatures. Phosphate loss during heating was 1.5–3.5% P_2O_5. No specific TGA peak could be attributed to P_2O_5 volatilisation and this probably occurred gradually with increasing temperature.

Estimated atmospheric emissions during vitrification showed considerable levels of CO_2 and low levels of SO_2, as discussed in Section 3.6. In addition the estimated emission of over 40 kg of HCl per tonne of waste B may be of concern. Evaluation of these emissions in the context of current EU environmental legislation, as discussed in the integrated pollution prevention and control guidance documents for the incineration of waste [10] indicated that if they were treated as such, both wastes could be safely processed within current atmospheric emissions limits. It is possible that abatement technology may be required in dealing with HCl generated from waste B. Waste P, which was regarded as more suitable for vitrification [1] also produced substantially lower emissions of CO_2 and SO_3, and zero HCl. If these wastes could be used in the immobilisation of yet other wastes, the compositional changes which this would introduce may allow immobilisation of higher levels of SO_3, as occurred with some phosphate glasses for nuclear waste [7,8]. As a result the atmospheric sulphate emissions would be even lower.

XRD results for the waste samples were discussed briefly in a previous publication [1]. An additional phase, $Zn_2P_2O_7$ was noted in samples B-3 and B-4, which had not previously been identified. Sample B-1 contained a mixture of crystalline $ZnFe_2O_4$ and Fe_3O_4. A variety of hydrocarbon compounds was also suggested by XRD spectra, but identification of specific molecules was not possible because of line broadening, which can indicate poor crystallisation. However, a higher level of crystallinity was evidenced by XRD for sample P-1. This difference may be a result of waste P originating from a single process and waste B deriving from a number of processes [1]. Heat treatment of sample B-1 to 1000 °C to make sample B-2 developed a third identifiable phase, ZnO, combusted the hydrocarbons and evolved HCl. Sample crystallinity was greatly increased by this treatment, as evidenced by XRD line narrowing. Addition of P_2O_5 to waste B created samples B-3 and B-4, which formed molten liquids at 1100 °C. $Zn_2P_2O_7$, $FePO_4$ and unidentified phase(s) formed during cooling of sample B-3. Sample B-4 developed $Zn_2P_2O_7$ and unidentified phase(s) during cooling. The behaviour of both samples was consistent with phosphate-deficient melts rich in zinc and iron. XRD also suggested the presence of $AlPO_4$ in samples B-3 and B-4 and it has been included in the list of identified phases. However, on the basis of the low aluminium contents of these samples, this is a tentative suggestion at best. Crystalline $Zn_2P_2O_7$ was developed from glasses similar to these by heat treatment [16]. Visual inspection of samples B-3 and B-4 showed increasing amorphous content with increasing P_2O_5 addition. This was consistent with our previous conclusion that addition of a slightly higher level of P_2O_5 than was made to form sample B-4, should allow formation of a fully amorphous phosphate glass from waste B [1].

The crystallisation behaviour of waste P exhibited an interesting trend with increasing P_2O_5 addition. XRD showed crystal phases in addition to an amorphous hump for samples P-2 and P-3. These partially crystallised samples both contained phases which we have attributed to a form of $AlPO_4$. The XRD spectrum for sample P-2 suggested the presence of Fe_2O_3. Addition of 10 wt.% P_2O_5 to sample P-2 to form sample P-3 resulted in the disappearance of the Fe_2O_3 phase and the occurrence of $FePO_4$ plus an unidentified phase. Sample P-4 was entirely amorphous. The presence of $AlPO_4$ in samples P-2 and P-3 was interesting, since this material contained relatively little Al_2O_3. However, the most easily crystallised phases, which formed when there was only a slight deficiency in phosphate, were $FePO_4$ and $AlPO_4$. With a further decrease in phosphate content, the $AlPO_4$ remained whilst the $FePO_4$ was replaced by Fe_2O_3. Therefore $AlPO_4$ formed when there was only a minor deficiency in phosphate but remained stable with further decreases in phosphate content. Clearly $AlPO_4$ formation is a sensitive indicator of the onset of phosphate deficiency in these glasses. Crystalline $AlPO_4$ has a structure and melting temperature analogous to some crystalline forms of SiO_2. Unlike iron phosphates, which have a wide glass formation region, aluminium phosphates only form stable glasses over a narrow range [42]. The addition of alkali oxides to aluminium phosphate increases the tendency for glass formation and reduces melting temperature, whilst maintaining an acceptably high chemical durability and allowing substantial levels of waste loading. For example, P_2O_5–Al_2O_3–Na_2O glasses have successfully been used in Russia for many years in the immobilisation of high level nuclear waste [43]. Since the chemical durability of sample P-2 was very similar to that of P-4, despite the presence of crystalline $AlPO_4$ and Fe_2O_3 [1], the crystallisation of $AlPO_4$ does not appear to cause the same order-of-magnitude decreases in chemical durability which occurred with crystallisation of some iron phosphate waste forms containing simulated nuclear waste [44]. Partial crystallisation of these vitrified wastes was therefore not considered to be a barrier to their use as immobilisation media [1].

DTA indicated that maximum crystallisation in waste B and P samples occurred in the range 635–675 °C, with a series of small peaks at 800–1000 °C due to melting of the

crystalline phases. The DTA results confirmed visual observations that at the melting temperatures of 1000 °C or 1100 °C which were used, all samples were fully liquid with no residual crystalline components. In general the behaviour was consistent with that of other phosphate glasses rich in iron [14,16,25,31]. The major DTA peak at 635–675 °C may be due to the formation of ferrous/ferric pyrophosphate, $Fe_3(P_2O_7)_2$ or $Fe^{2+}Fe^{3+}{}_2(P_2O_7)_2$ [14,25], or to similar Q^0, Q^1 and Q^2 crystalline species (where Q = number of bridging oxygens bonds per PO_4 group) [28]. It may also be due to the formation of $FePO_4$, as occurred during heat treatment of P_2O_5–Fe_2O_3–Na_2O glasses in oxygen [45] and P_2O_5–Fe_2O_3 glasses in argon [46]. In addition to the chemical composition, the $Fe^{2+}/\sum Fe$ redox ratio can influence the temperature at which crystallisation occurs [14,16,25,31,46], and increasing the $Fe^{2+}/\sum Fe$ ratio can reduce crystallisation temperature [46]. It is therefore important, in order to optimise high temperature glass stability, to have a low $Fe^{2+}/\sum Fe$ ratio. Iron in samples P-4 and B-4 was confirmed by Mössbauer spectroscopy to occur predominantly as Fe^{3+} ions. However, these samples had different chemical compositions, which affected crystallisation behaviour more strongly than the relatively small differences in redox ratio. There was some evidence of very weak exothermic DTA peaks in the region of 800 °C, as occurred with some binary iron phosphate glasses [14,25,31] and a zinc-iron phosphate glass [16]. These peaks had been attributed to ferric pyrophosphate, $Fe_4(P_2O_7)_3$, the formation of which was strongly dependent upon redox [14,25]. The presence of these weak peaks for samples B-4, P-2, and P-4 may indicate the formation of very small amounts of such phases, however, the oxidised nature of the iron would have prevented their formation at meaningful levels.

Values of T_g for samples B-4, P-2 and P-4 were consistent with those obtained for similar phosphate glasses [6,7,14,16,25]. Sample P-4 exhibited T_g ~505 °C, a crystallisation onset temperature T_x of ~595 °C with maximum crystallisation temperature T_c at ~650 °C, and a liquidus temperature T_{liq} of ~930 °C. In order to evaluate the waste samples against a benchmark, the DTA trace of "MW", a borosilicate glass detailed previously [1], was measured. Its T_g was ~530 °C, T_c ~695 °C and T_{liq} ~900 °C. The flat, featureless nature of its DTA trace was indicative of very high thermal stability, whereas iron phosphate-type glasses have a greater tendency to crystallise. The temperature difference $T_x - T_g$ is proportional to the glass-forming tendency which is itself proportional to the thermal stability of the glass [47]. Glass MW had the highest glass forming tendency of the samples measured, with $T_x - T_g \approx 120$ °C, but the fully amorphous sample P-4 also demonstrated good glass-forming tendency with $T_x - T_g \approx 90$ °C. The waste glasses also exhibited stronger exothermic and endothermic behaviour than glass MW, which is consistent with lower thermal stability.

Crystallised lead-iron phosphate glasses exhibited narrower infrared absorption bands than their fully vitreous counterparts and this was attributed to higher local symmetry in the crystalline regions [18]. However, band positions did not change with crystallisation, and it was suggested that the sample had retained its local structure in terms of contributing phosphate species [18]. It was therefore expected that the FTIR spectra for each sample examined in this study, except P-4, would have both amorphous and crystalline contributions. For waste P samples, sample P-2 exhibited the greatest visible levels of crystallinity, P-3 less and P-4 none, and although FTIR band widths and intensities may have changed, band wavenumbers did not shift substantially. Fig. 5 clearly shows band narrowing for the most crystalline sample, P-2. Absorption bands occurred for sample P-2 at 470, 545, 595, 650, 750, 950, 1020, 1060 and 1095 cm^{-1}. A very weak, broad absorption at ~1200–1300 cm^{-1} occurred in P-3 and P-4. Broadening, caused by a wider distribution of site parameters, made it difficult to fully interpret some absorption bands in the more glassy samples P-3 and P-4. Spectral deconvolution would be required for their full assessment [13,23]. However, the presence of well-defined bands in sample P-2 indicated their expected positions in the other samples. Broad absorption bands were found at ~1020 cm^{-1} and 1050–1150 cm^{-1} with the weak, broad band at 1200–1300 cm^{-1} in spectra for samples B-3, B-4, P-3 and P-4. Assessment of a wide range of IR spectra indicated that as a general rule, the frequency of IR absorption bands in phosphate glasses of similar composition to ours, increases with increasing Q-value, albeit with a dependence upon the type of vibration [4,6,8,13–31]. This could explain the change in the overall profile of spectra P-2 through P-4. The peak maximum near 1100 cm^{-1} became broadened and moved to higher frequencies with increasing P_2O_5 content. Strengthening of the high frequency band at 1200–1250 cm^{-1} and a clear change in the character of the main peak at 1020–1150 cm^{-1} also occurred. The constituent peaks within this main peak have widely been attributed to various vibrations of Q^0 $(PO_4)^{3-}$, Q^1 $(PO_3)^{2-}$ and Q^2 $(PO_2)^-$ groups, with frequencies of vibration roughly occurring in the order $Q^3 > Q^2 > Q^1 > Q^0$ through the range 1400–950 cm^{-1}. Not all literature sources are in agreement, however, a general trend does appear to exist [4,6,8,13–31].

An absorption band at 1200–1300 cm^{-1} has been attributed by some to P=O bonds in Q^3 phosphate groups [6,26]. Such bonds are known to exhibit a characteristic absorption in the range 1250–1400 cm^{-1} [6,17–21,26,27], however, there are other sites which may also give rise to such an absorption. Ding et al. [27] noted an overlap in absorption frequencies due to Q^3 P=O bonds and Q^2 $(PO_2)^-$ groups. The P=O bond is opened upon addition of sufficient Fe_2O_3, forming covalent P–O–Fe bonds [21,26]. In waste B and P samples this absorption band was very weak, and was substantially masked by the tails of the stronger bands occurring at lower wave numbers. However, the addition of P_2O_5 to waste P samples appeared to strengthen the absorption at 1200–1300 cm^{-1}, particularly for sample P-4, where a change in the spectral gradient was visible. We suggest that this may indicate the formation of more Q^2 and/or Q^3

units, and it is consistent with the other evidence for partial re-polymerisation of these glasses. It also suggests that the number of P=O bonds was still low, even in the most polymerised samples. Karabulut et al. [20] carried out Q-value site estimations for P_2O_5–FeO glasses, based on previous work by Hoppe [48]. At 50 mol% FeO (~37 wt.% Fe_2O_3) in binary iron phosphate glasses, no Q^3 sites of any type were expected to exist, assuming Fe ions were in octahedral coordination and coordinated only by terminal oxygens. This was further evidence that for our spectra, the IR absorption band near 1250 cm^{-1} was more likely to be attributable to Q^2 sites than to Q^3 sites owing to the expected relative abundances of these two types of site.

Two characteristic and well-defined FTIR absorption bands occurred in all spectra at approximately 750 cm^{-1} and 950 cm^{-1}. These are widely attributed to symmetric and asymmetric stretching vibrations of the P–O–P bridges [4,6,13–17,19,20,22,23,26–28,30]. However, there is some disagreement on the issue: a band at 950 cm^{-1} has also been attributed to Q^0 $(PO_4)^{3-}$ groups [7,25]. In our samples the strengths of the two absorption bands at 750 cm^{-1} and 950 cm^{-1} increased proportionately to one another throughout the series P-2 to P-4, i.e. with increasing P_2O_5 content of the glass. It therefore seems more likely that these absorption bands originate from the same source, for example if they are due to symmetric and asymmetric vibrations of P–O–P bonds. Assuming this is the case, the number of P–O–P bonds increased upon addition of 10 and 20 wt.% P_2O_5. The absorption band at 1020 cm^{-1}, clearly visible in all spectra even when it was surrounded by the large, broad peak near 1100 cm^{-1}, appeared to decrease in strength with increasing P_2O_5 content. If this band is due to Q^0 $(PO_4)^{3-}$ groups as some have suggested [8,21,23,24,27], then it indicates an increase in the number of P–O–P bonds at the expense of Q^0 sites. It can therefore be argued that the ratio of Q^1 $(P_2O_7)^{4-}$ dimers to Q^0 $(PO_4)^{3-}$ monomers increases through the sample series P-2 to P-4. The appearance of a broad band near 1250 cm^{-1} may also indicate the presence of more Q^2 $(PO_3)^{2-}$ groups, so the monomer PO_4 groups may be replaced by a mixture of short-chain groups, for example dimers and trimers.

Absorption bands in the range 400–600 cm^{-1} have been attributed mainly to vibrations of Q^0 $(PO_4)^{3-}$ groups [6,19,21,22] or Q^1 $(P_2O_7)^{4-}$ dimers [14–16,24,25] which overlap vibrations of Fe–O bonds and Zn–O bonds. With the addition of P_2O_5 through samples P-2 to P-4, the strength of the band at 515 cm^{-1} grew, whilst the bands at ~595 cm^{-1} and ~650 cm^{-1} disappeared. This can be attributed to a combination of changes in the relative abundance of Q^0, Q^1 and Q^2 species and line broadening due to decreasing levels of crystallinity. Overall these results strongly suggest that the structural units of the glasses consist of Q^0, Q^1 and Q^2 species but with few or no Q^3 groups. Addition of P_2O_5 through series P-2 to P-4 resulted in an increase in the average Q-value. These glasses were composed largely of Q^0 $(PO_4)^{3-}$ and Q^1 $(PO_3)^{2-}$ groups, with some Q^2 $(PO_2)^{-}$ groups also present.

Comparison of the spectra for waste B with waste P samples indicated that they had very similar structures, however, some differences did exist. The absorption bands near 750 cm^{-1} and 950 cm^{-1} were weaker and less well-defined for waste B samples, whereas the main band near 1100 cm^{-1} was broader. In particular the ~1020 cm^{-1} component of this main band was stronger in the waste B samples. Using the band assignments discussed previously, this indicated that fewer P–O–P bonds were present but the phosphate groups had a lower average Q-value. The higher ($ZnO + Fe_2O_3$) content of waste B glasses would be expected to de-polymerise the material more strongly, leading to increased numbers of Q^0 and Q^1 groups. Like sample P-2, samples B-3 and B-4 exhibited absorption bands at 545 cm^{-1}, 595 cm^{-1} and 650 cm^{-1}. Line narrowing due to crystallinity may have played a role, however, similar effects occurred for a series of amorphous P_2O_5–Fe_2O_3–ZnO glasses with increasing iron/zinc ratio at a fixed P_2O_5 content [16].

Chemical durability of ternary P_2O_5–Fe_2O_3–ZnO glasses improves by four orders of magnitude as ZnO is replaced by Fe_2O_3 [6,16]. The iron contents of vitrified wastes B and P were therefore crucial to their high chemical durability. However, zinc phosphate glasses can have acceptable chemical durability, higher than several other phosphate systems [49]. Zinc in vitrified wastes B and P would contribute to the general depolymerisation of the phosphate network [49,50]. Divalent cations such as Zn^{2+} and Ca^{2+} can form ionic crosslinks between the non-bridging oxygens in different phosphate chains, improving chemical durability [49,50]. Recent results discussed by Tischendorf et al. [49] indicated strongly that in highly depolymerised phosphate glasses such as our vitrified wastes, Zn^{2+} ions are 5- or 6-coordinated.

Room temperature fitted Mössbauer hyperfine parameters were consistent with those for glasses based on iron phosphate [14,20], lead-iron phosphate [18], sodium-iron phosphate [45], zinc-iron phosphate [16] and complex iron phosphate glasses containing several cations [4,7,22]. Our fitted parameters were in particularly good agreement with those for surrogate waste-loaded multi-component iron phosphate glasses [7,8,22] compared with laboratory glasses containing relatively few components. Values of CS and QS both indicated that Fe^{2+} and Fe^{3+} ions occupied distorted octahedral sites. Linewidths indicated a range of site distortions, as would be expected in an amorphous material.

The majority of the more recent studies involving Mössbauer spectroscopy of iron-containing phosphate glasses have assumed the recoil-free fractions of Fe^{2+} and Fe^{3+} ions were equal at room temperature [4,7–9,14,16,18,20,45]. However, specific Mössbauer studies on several different iron-containing phosphate glasses have shown that this is not the case [32–35]. These studies found that recoil-free fraction for Fe^{3+} was 1.25–1.35 times the recoil-free fraction for Fe^{2+} ions. As a result, a factor of 1.30 was used in our work when estimating the redox ratio from area ratios. Redox was moderately different for the two samples studied by Mössbauer. Sample P-4 contained

11.2% of total iron present as Fe^{2+} whereas sample B-4 was more reduced, with 18.4% of the total iron as Fe^{2+}. The fitted Mössbauer parameters for Fe^{3+} ions, the predominant iron species in these samples, were identical for both samples within the limits of error. This indicated that iron plays an identical role in these glass structures and exists in very similar environments, i.e. distorted octahedral sites with the same range of distortions. Owing to the differences in composition between the glasses, this was strong evidence for the structural insensitivity of these glasses to compositional change, a property which makes iron phosphate based glasses particularly promising as hosts for the immobilisation of toxic and nuclear wastes.

5. Conclusions

Atmospheric emissions of CO_2 and SO_3 during high temperature processing of wastes were estimated to be below legal limits for high volume processing, although HCl emission from waste B may be of concern. The decomposition of iron and zinc sulphates and the emission of CO_2 were thought to be related to specific TGA peaks. Only one sample, P-4, was entirely amorphous; all others contained some crystallinity. The formation of crystalline $AlPO_4$ in waste P samples was a sensitive indicator of phosphate deficiency of this material in terms of glass formation. Other identified phases included $FePO_4$ and Fe_2O_3 in waste P samples and $Zn_2P_2O_7$ and $FePO_4$ in waste B samples. Crystallisation of vitrified wastes occurred at 635–675 °C, and T_g occurred at 450–500 °C. Glass thermal stability was not as good as that of MW, a borosilicate glass used for nuclear waste vitrification, but the thermal stability was still considered to be good. Iron occurred in distorted octahedral sites in the vitrified waste forms, predominantly as Fe^{3+} ions, with $Fe^{2+}/\sum Fe$ being less than 20%. Glasses and partially crystallised glasses were highly de-polymerised, with phosphate occurring as very short chain units being largely present as monomers and dimers.

References

[1] P.A. Bingham, R.J. Hand, Vitrified metal finishing wastes. i. Composition, density and chemical durability, J. Hazard. Mater. B119 (2005) 125–133.

[2] P. Colombo, G. Brusatin, E. Bernardo, G. Scarinci, Inertization and reuse of waste materials by vitrification and fabrication of glass-based products, Curr. Opin. Sol. State Mater. Sci. 7 (2003) 225–239.

[3] G. Scarinci, G. Brusatin, L. Barbieri, A. Corradi, I. Lancellotti, P. Colombo, S. Hreglich, R. Dall'Igna, Vitrification of industrial and natural wastes with production of glass fibres, J. Eur. Ceram. Soc. 20 (2000) 2485–2490.

[4] M. Karabulut, E. Melnik, R. Stefan, G.K. Marasinghe, C.S. Ray, C.R. Kurkjian, D.E. Day, Mechanical and structural properties of phosphate glass, J. Non-Cryst. Solids 288 (2001) 8–17.

[5] OSWER Innovations Pilot: Industrial phosphate sludge waste as a raw material for iron phosphate glass, EPA 500-F-03-008, 2003, http://www.epa.gov/oswer/docs/iwg/Phosphatefinal.pdf.

[6] T. Jermoumi, M. Hafid, N. Niegisch, M. Mennig, A. Sabir, N. Toreis, Properties of $(0.5-x)Zn-xFe_2O_3-0.5P_2O_5$ glasses, Mater. Res. Bull. 37 (2002) 49–57.

[7] C.W. Kim, D.E. Day, Immobilisation of Hanford LAW in iron phosphate glasses, J. Non-Cryst. Solids 331 (2003) 20–31.

[8] C.W. Kim, C.S. Ray, D. Zhu, D.E. Day, D. Gombert, A. Aloy, A. Mogus-Milankovic, M. Karabulut, Chemically durable iron phosphate glasses for vitrifying sodium bearing waste (SBW) using conventional and cold crucible induction melting (CCIM) techniques, J. Nucl. Mater. 322 (2003) 152–164.

[9] S.T. Reis, M. Karabulut, D.E. Day, Structural features and properties of lead-iron-phosphate nuclear wasteforms, J. Nucl. Mater. 304 (2002) 87–95.

[10] Integrated pollution prevention and control (IPPC), guidance for the incineration of waste and fuel manufactured from or including waste, http://www.environment-agency.gov.uk/yourenv/consultations/530870/.

[11] J.M. Williams, J.S. Brooks, Thickness dependence of Mössbauer absorption line areas in unpolarised and polarised absorbers, Nucl. Instrum. Methods 128 (1975) 368–372.

[12] K. Lagrec, D.G. Rancourt, Recoil: Mössbauer spectral analysis software for windows, 1998, http://www.physics.uottawa.ca/~recoil/.

[13] A.M. Efimov, Vibrational spectra, related properties, and structure of inorganic glasses, J. Non-Cryst. Solids 253 (1999) 95–118.

[14] C.S. Ray, X. Fang, M. Karabulut, G.K. Marasinghe, D.E. Day, Effect of melting temperature and time on iron valence and crystallisation of iron phosphate glasses, J. Non-Cryst. Solids 249 (1999) 1–16.

[15] X. Fang, C.S. Ray, G.K. Marasinghe, D.E. Day, Properties of mixed Na_2O and K_2O iron phosphate glasses, J. Non-Cryst. Solids 263–264 (2000) 293–298.

[16] S.T. Reis, M. Karabulut, D.E. Day, Chemical durability and structure of zinc-iron phosphate glasses, J. Non-Cryst. Solids 292 (2001) 150–157.

[17] A. Mogus-Milankovic, A. Satic, S.T. Reis, K. Furic, D.E. Day, Mixed ion-polaron transport in Na_2O–PbO–Fe_2O_3–P_2O_5 glasses, J. Non-Cryst. Solids 342 (2004) 97–109.

[18] S.T. Reis, D.L.A. Faria, J.R. Martinelli, W.M. Pontuschka, D.E. Day, C.S.M. Partiti, Structural features of lead iron phosphate glasses, J. Non-Cryst. Solids 304 (2002) 188–194.

[19] A. Chahine, M. Et-tabirou, M. Elbenaissi, M. Haddad, J.L. Pascal, Effect on the structure and properties of $(50-x/2)Na_2O$–$xCuO$–$(50-x/2)P_2O_5$ glasses, Mater. Chem. Phys. 84 (2004) 341–347.

[20] M. Karabulut, E. Metwalli, D.E. Day, R.K. Brow, Mössbauer and IR investigations of iron ultraphosphate glasses, J. Non-Cryst. Solids 328 (2003) 199–206.

[21] M. Hafid, T. Jeroumi, N. Niegisch, M. Mennig, Thermal and infrared characterisation of new barium-iron-metaphosphate glasses, Mater. Res. Bull. 36 (2001) 2375–2382.

[22] B. Samuneva, P. Tzvetkova, I. Gugov, V. Dimitrov, Structural studies of phosphate glasses, J. Mater. Sci. Lett. 15 (1996) 2180–2183.

[23] A.M. Efimov, IR fundamental spectra and structure of pyrophosphate glasses along the $2ZnO{\cdot}P_2O_5$–$2Me_2O{\cdot}P_2O_5$ join (Me being Na and Li), J. Non-Cryst. Solids 209 (1997) 209–226.

[24] G. Guo, Y. Chen, Thermal analysis and infrared measurements of a lead-barium-aluminium phosphate glass, J. Non-Cryst. Solids 201 (1996) 262–266.

[25] X. Fang, C.S. Ray, A. Mogus-Milankovic, D.E. Day, Iron redox equilibrium, structure and properties of iron phosphate glasses, J. Non-Cryst. Solids 283 (2001) 162–172.

[26] T. Jermoumi, M. Hafid, N. Toreis, Density, thermal and FTIR analysis of $(50-x)BaO{\cdot}xFe_2O_3{\cdot}50P_2O_5$ glasses, Phys. Chem. Glasses 43 (2002) 129–132.

[27] J.S. Ding, S.W. Yung, P.Y. Shih, Effect of Al_2O_3 on properties and structure of lead zinc phosphate glasses, Phys. Chem. Glasses 43 (2002) 300–305.

[28] M. El Hezzat, M. Et-tabirou, L. Montagne, G. Palavit, A. Mazzah, P. Dhamelincourt, Spectroscopic studies of the structure of Na_2O-CdO-PbO-P_2O_5 metaphosphate glasses, Phys. Chem. Glasses 44 (2003) 345–348.
[29] E.B. Araujo, J.A. Eiras, E.F. de Almeida, J.A.C. De Paiva, A.S.B. Sombra, Structure and nucleation mechanism of the iron lithium niobium phosphate glasses studied by infrared spectroscopy and DTA, Phys. Chem. Glasses 40 (1999) 273–276.
[30] M. Abid, M. Elmoudane, M. Et-tabirou, Spectroscopic studies of the structure of sodium lead oligophosphate glasses, Phys. Chem. Glasses 43 (2002) 267–270.
[31] A. Mogus-Milankovic, M. Rajic, A. Drasner, R. Trojko, D.E. Day, Crystallisation of iron phosphate glasses, Phys. Chem. Glasses 39 (1998) 70–75.
[32] H. Itoh, T. Inamura, H. Wakabayashi, T. Toriyama, H. Iijima, Mössbauer spectroscopy on an alkali phosphate $20Na_2O$–$20Fe_2O_3$–$60P_2O_5$ glass at low temperature, ICAME-95 (1996) 445–448.
[33] T. Inamura, H. Wakabayashi, T. Toriyama, H. Iijima, T. Tsuchiya, Mössbauer spectroscopy of a semiconductive phosphate glass ($10MnO$–$30Fe_2O_3$–$60P_2O_5$) at low temperature, ICAME-95 (1996) 405–408.
[34] T. Oohata, K. Shirahata, T. Toriyama, T. Inamura, K. Yoshino, H. Iijima, Mössbauer spectroscopy of a semiconductive phosphate glass ($10V_2O_5$–$30Fe_2O_3$–$60P_2O_5$) at low temperature, Hyperfine Interact. 94 (1994) 2131–2136.
[35] J.S. Brooks, G.L. Williams, D.W. Allen, Variable temperature ^{57}Fe Mössbauer studies of some phosphate glasses, Phys. Chem. Glasses 33 (1992) 171–176.
[36] C.R. Kurkjian, Mössbauer spectroscopy in inorganic glasses, J. Non-Cryst. Solids 3 (1970) 157–194.
[37] G. Zheng, J.A. Kozinski, Thermal events occurring during the combustion of biomass residue, Fuel 79 (2000) 181–192.
[38] A.N. Garcia, A. Marcilla, R. Font, Thermogravimetric kinetic study of the pyrolysis of municipal solid waste, Thermochim. Acta 254 (1995) 277–304.
[39] C.-H. Wu, C.-Y. Chang, C.-H. Tseng, Pyrolysis products of uncoated printing and writing paper of MSW, Fuel 81 (2002) 719–725.
[40] D.C.R. Espinosa, J.A.S. Tenorio, Thermal behaviour of chromium electroplating sludge, Waste Manage. 21 (2001) 405–410.
[41] R.V. Siriwardane, J.A. Poston, E.P. Fisher, M.-S. Shen, A.L. Miltz, Decomposition of the sulphates of copper, iron(II), iron(III), nickel, and zinc: XPS, SEM, DRIFTS, XRD, and TGA study, Appl. Surf. Sci. 152 (1999) 219–236.
[42] H. Rawson, Inorganic Glass-Forming Systems, Academic Press, London, 1967.
[43] I.W. Donald, B.L. Metcalfe, R.N.J. Taylor, Review: the immobilisation of high level radioactive wastes using ceramics and glasses, J. Mater. Sci. 32 (1997) 5851–5887.
[44] D.E. Day, Z. Wu, C.S. Ray, P. Hrma, Chemically durable iron phosphate glass wasteforms, J. Non-Cryst. Solids 241 (1998) 1–12.
[45] A. Mogus-Milankovic, D.E. Day, G.J. Long, G.K. Marasinghe, Structural and magnetic properties of Fe_2O_3–P_2O_5–Na_2O glasses. Part. I. Oxygen heat treatment, Phys. Chem. Glasses 37 (1996) 57–61.
[46] J. Doupovec, J. Sitek, J. Kakos, Crystallisation of iron phosphate glasses, J. Therm. Anal. 22 (1981) 213–219.
[47] A. Hruby, Evaluation of glass-forming tendency by means of DTA, Czech. J. Phys. B 22 (1972) 1187–1193.
[48] U. Hoppe, A structural model for phosphate glasses, J. Non-Cryst. Solids 195 (1996) 138–147.
[49] B. Tischendorf, J.U. Otaigbe, J.W. Wiench, M. Pruski, B.C. Sales, A study of short and intermediate range order in zinc phosphate glasses, J. Non-Cryst. Solids 282 (2001) 147–158.
[50] B.C. Bunker, G.W. Arnold, J.A. Wilder, Phosphate glass dissolution in aqueous solutions, J. Non-Cryst. Solids 64 (1984) 291–316.